A novel class of protease targets of phosphatidylethanolamine-binding proteins (PEBP): a study of the acylpeptide hydrolase and the PEBP inhibitor from the archaeon *Sulfolobus solfataricus*†

Gianna Palmieri,‡[a] Emma Langella,‡[b] Marta Gogliettino,[a] Michele Saviano,*[bc] Gabriella Pocsfalvi[a] and Mose Rossi[d]

Received 5th May 2010, Accepted 13th August 2010
DOI: 10.1039/c005293k

This work describes the identification and characterization of a *Sulfolobus solfataricus* acylpeptide hydrolase, named $APEH_{Ss}$, recognised as a new protease target of the endogenous PEBP inhibitor, SsCEI. APEH is one of the four members of the prolyl oligopeptidase (POP) family, which removes acylated amino acid residues from the N terminus of oligopeptides. $APEH_{Ss}$ is a cytosolic homodimeric protein with a molecular mass of 125 kDa. It displays a similar exopeptidase and endopeptidase activity to the homologous enzymes from *Aeropyrum pernix* and *Pyrococcus horikoshii*. Herein we demonstrate that SsCEI is the first PEBP protein found to efficiently inhibit APEH from both S. *solfataricus* and mammalian sources with IC_{50} values in the nanomolar range. The 3D model of $APEH_{Ss}$ shows the typical structural features of the POP family including an N-terminal β-propeller and a C-terminal α/β hydrolase domain. Moreover, to gain insights into the binding mode of SsCEI toward $APEH_{Ss}$, a structural model of the inhibition complex is proposed, suggesting a mechanism of steric blockage on substrate access to the active site or on product release. Like other POP enzymes, APEH may constitute a new therapeutic target for the treatment of a number of pathologies and this study may represent a starting point for further medical research.

Introduction

The I51 serine protease inhibitor family shows no sequence similarity to other known proteinase inhibitors and is characterized by the presence of a phosphatidylethanolamine binding (PEB) domain.[1] The PEBP (PEB protein) family consists of over 500 multifunctional proteins, which are involved in signalling mechanisms during cell growth and/or differentiation *via* modulation of kinase or serine protease activities.[2–4] Among the PEBPs belonging to the I51 inhibitor family, the TFS1 from *Saccharomyces cerevisiae*[5] and the mouse PEBP[1] are considered to be the archetypal serine proteinase inhibitors.

Recently SsCEI (*Sulfolobus solfataricus* chymotrypsin-elastase inhibitor), a new PEBP protein of the I51 inhibitor class, has been purified from the archaeon hyperthermophile *S. solfataricus*.[6] SsCEI efficiently inhibits bovine α-chymotrypsin and porcine elastase *in vitro* but not trypsin, a distinguishing feature of all members of the I51 family. Point mutation experiments allowed the identification of the "reactive site loop" located on the surface at the C-terminal region of SsCEI and responsible for the interaction with eukaryal protease targets. This loop includes a new sequence motif seen for the first time in chymotrypsin-like enzyme inhibitors.[6]

In order to further study the biological function of SsCEI, we isolated its endogenous target enzyme, a serine protease belonging to the acylpeptide hydrolase (APEH) family. APEH, also referred to as acylaminoacyl peptidase or acylaminoacyl peptide hydrolase, represents one of the four members of the prolyl oligopeptidase (POP, clan SC, family S9) class.[7–9] POP is a relatively new group of serine peptidases able to hydrolyze relatively short peptide substrates and showing a canonical α/β hydrolase fold together with the Ser-Asp-His catalytic triad that is covered by an unusual β-propeller.[10–13] Specifically, APEH catalyzes the removal of a N-acylated amino acid from blocked peptides, producing an acylamino acid and a peptide with a free N-terminus shortened by one amino acid residue.[9] So far, these enzymes have been found in a number of eukaryal[14,15] organisms and in some Archaea[12,16] but never in prokaryotes. Rat,[17] porcine,[18] human[19] and bovine[14,15] APEHs from different tissues, including blood, brain and

[a] *Institute of Protein Biochemistry, IBP-CNR, Napoli, Italy*
[b] *Institute of Biostructures and Bioimaging, IBB-CNR, via Mezzocannone, 16, 80134, Napoli, Italy. E-mail: msaviano@unina.it; Fax: + 39-0812534560; Tel: + 39-0812536648*
[c] *Institute of Crystallography, IC-CNR, Bari, Italy*
[d] *Department of Structural and Functional Biology, University of Naples "Federico II", Napoli, Italy*

† Electronic supplementary information (ESI) available: SDS-PAGE of purified SSCEI-interacting protease and standard curve to determinate molecular weight; graphs concerning the effect of pH, $CaCl_2$, SDS and temperature on $APEH_{Ss}$ activity and the binding of SsCEI to APEHs from porcine liver and *Sulfolobus solfataricus*; Figures of the $APEH_{Ss}$ model potential energy surface and of the predicted complex between the $APEH_{Ss}$ dimer model and two SsCEI molecules; Table of peptide details on protease identification. See DOI: 10.1039/c005293k

‡ These authors contributed equally to the work

liver, show significant sequence identity and are reported to form homotetramers. Moreover, APEH has been characterized from hyperthermophile *Aeropyrum pernix* K1,[12] whose crystal structure has also been resolved,[13] and from the thermophilic archaeon *Pyrococcus horikoshii* OT3.[16]

Like other POP enzymes, APEHs are believed to be important targets for drug design. Whilst human APEH is known to be deficient in small-cell lung and renal carcinomas, a role in the malignant state of these cell lines has not so far been established.[20–22] Furthermore, porcine brain APEH was found to be potently inhibited by organophosphorous compounds and it has been proposed as a new pharmacological target for the cognitive-enhancing effects of these compounds in the treatment of neurodegenerative diseases.[23]

The aim of the present work was the isolation of the endogenous protease target of SsCEI, and the analysis of the protease/SsCEI interaction from a biochemical/structural point of view. *In vitro* inhibition studies showed that the isolated SsCEI was the first protein inhibitor able to efficiently interact with APEHs from different mammalian sources. In addition, the availability of the crystal structure of $APEH_{Ap}$ from *A. pernix*,[12,13] which shares a significant sequence identity (34%) with APEH from *S. solfataricus*, prompted us to undertake a molecular modelling study in order to obtain a more complete picture of the enzyme structure as well as of its interaction with the SsCEI inhibitor at the atomic level. The results obtained represent an important step in clarifying the biological and evolutionary roles of the PEBP protease inhibitors such as SsCEI, and their interaction with a new class of enzyme target belonging to APEH family.

Materials and methods

Strains, media and growth conditions

Sulfolobus solfataricus strain P2 (DSM 1617) was grown aerobically at 80 °C in Brock's basal salt medium containing 0.05% yeast extract (Bacto), 0.2% tryptone (Bacto), 0.2% sucrose (TYS medium) and buffered at pH 3.5 with sulfuric acid 10%. Growth of cells was monitored by measuring the OD at 600 nm. The culture media was harvested at the stationary phase (1.3 OD) and cells were recovered by centrifugation and stored at −20 °C until use.

Enzyme purification

Enzyme purification was followed using Succinyl-Glycine-Glycine-Phenylalanine-*p*-nitroanilide (Suc-GlyGlyPhe-*p*NA) as substrate. The cell pellet from 0.5 L of *S. solfataricus* culture, was resuspended in TEK buffer (20 mM Tris-HCl, 0.1 mM EDTA, 120 mM KCl, pH 7.5) containing 0.1% Triton-100, and the mixture was incubated for 30 min on ice. The suspension was centrifuged at 15 000 × g for 50 min at 4 °C. The supernatant containing the soluble protease was dialyzed against 25 mM Tris-HCl, 1.5 M ammonium sulfate, pH 7.5 and loaded onto a Phenyl Sepharose column (1.6 × 2.5 cm) (Amersham Biosciences) connected to an $AKTA_{FPLC}$ system (Amersham Biosciences) equilibrated with the same buffer. Bound proteins were eluted with a linear gradient of Tris-HCl 25 mM buffer, pH 7.5 (0–100%) at a flow rate of 1 mL min^{-1}. The active fractions were pooled and then applied to a Mono Q 5/50 column (5 × 50 mm) (Amersham Biosciences) connected to $AKTA_{FPLC}$ system (Amersham Biosciences) and equilibrated with buffer Tris-HCl 25 mM, pH 7.5 (buffer A). Proteins were eluted with a linear ionic gradient from 0 to 0.5 M NaCl in buffer A at a flow rate of 1 mL min^{-1}. The active fractions were pooled, dialyzed against 25 mM Tris-HCl buffer, pH 7.5 and concentrated by ultrafiltration. The concentrated sample was applied to a Superose 12 HR 10/30 column (Pharmacia Biotech) and eluted with 25 mM Tris-HCl buffer, pH 7.5, containing 50 mM NaCl at a flow rate of 1 mL min^{-1}. The active fractions eluted were pooled and dialyzed against 25 mM Tris- HCl, 1.5 M ammonium sulfate buffer, pH 7.5 (buffer B) and loaded onto a Phenyl Superose PC 1.6/5 connected to a SMART System (Pharmacia) equilibrated in buffer B. Bound proteins were eluted with a linear gradient of 25 mM Tris-HCl pH 7.5 (0–100%). Active fractions were pooled and the purified protease was stored at 20 °C in 25 mM Tris-HCl buffer, pH 7.5 containing 5% glycerol.

Molecular mass determination

Protein homogeneity was estimated by SDS-PAGE using 8.0% (w/v) acrylamide resolving gel. Standard proteins (Broad Range) were from New England BioLabs. Molecular mass of the native enzyme was determined using a Superose 12 HR 10/30 column, calibrated with molecular mass markers: thyroglobulin (670 000 Da), bovine γ-globulin (158 000 Da), chicken ovalbumin (44 000 Da), equine myoglobin (17 000 Da) and vitamin B_{12} (1350 Da) (BioRad). Native molecular mass determination of purified protease was also performed by using a Superdex 200 PC 3.2/30 column connected to the a SMART System. The calibration of the column was performed using the molecular mass standards described above.

Nano-HPLC-MS/MS analysis

The protein band of interest, stained with Coomassie Brilliant Blue G250, was excised from a preparative SDS-PAGE (8.0%) (20 × 20 cm) and *in-gel* digestion was performed according to Shevchenko *et al.*[24] Peptide mixture was analyzed by a quadrupole time of flight instrument (Q-Star Elite, Applied Biosystems) coupled online to a nano-HPLC system (Ultimate 3000, Dionex). Sample (5 µl out of 40 µl) was concentrated and desalificated using a C18 reverse-phase trap column, PepMap, 5 mm length, 300 Å, (LCPackings, Sunnyvale, CA USA) by 2% acetonitrile in 0.1% formic acid and 0.025% trifluoroacetic acid at 30 µl min^{-1} flow rate for 5 min. Peptides were then separated by a C18 reverse-phase capillary column, 15 cm length, 75 µm ID, 300 Å (LCPackings, Sunnyvale, CA USA), at a flow rate of 300 nL min^{-1} using a linear gradient of eluent B (98% acetonitrile in 0.1% formic acid and 0.025% trifluoro-acetic acid) in A (2% acetonitrile in 0.1% formic acid and 0.025% trifluoroacetic acid) from 5 to 50% in 30 min. Pulled silica capillary (170 µm outer diameter/100 µm internal diameter, tip 30 µm internal diameter) was used as nanoflow tip. Collision induced dissociation experiments were carried out in information dependent acquisition (IDA) mode in the range of m/z 70 to 1500. Nitrogen was used as collision gas.

Precursor ions were chosen as the two most intense peaks of each MS1 scan. Dynamic collision energy depending on the mass and the charge of the precursor ion was applied. Raw data were analysed and peak list was generated by Analyst QS 2.0 software (Applied Biosystems). MASCOT Server v. 2.2 was used for protein identification and set up to search the NCBInr database with Archaea (Archaeobacteria) (134 034 sequences) taxonomy. Trypsin was specified as the digestion enzyme with a maximum of one missed cleavage site. Mascot was run with a fragment ion mass tolerance of 0.08 Da and a parent ion tolerance of 50 ppm. The carbamidomethyl derivative of cysteine was specified as a fixed modification while oxidation of methionine was specified as variable modification in a Mascot search. Two independent nano-HPLC-ESI-MS/MS experiments were performed.

N-Terminal amino acid sequence analysis

The purified protease was subjected to automated Edman degradation, using a Perkin-Elmer Applied Biosystem 477A pulsed-liquid protein sequencer. The sequence database was searched using the BLAST-PSI program. Multiple sequence alignments and identity scores were generated by the CLUSTALW program.

Protease activity assays

The endopeptidase activity of APEH was measured spectrophotometrically following the release of *p*-nitroanilide (*p*NA) from the chromogenic substrate Suc-GlyGlyPhe-*p*NA (Bachem). The reaction mixture (1 mL) containing the appropriate amount of enzyme in 25 mM Tris-HCl buffer, pH 7.5, was preincubated at 80 °C for 2 min. Then, 0.1 mM Suc-GlyGlyPhe-*p*NA was added and the release of *p*-nitroanilide (ε_{410} = 8800 M^{-1} cm^{-1}) was measured by recording the absorbance increase at 410 nm on a Cary 100 SCAN (VARIAN) UV/Vis spectrophotometer, equipped with a thermostated cuvette compartment. One unit of APEH activity (U) is defined as the amount of enzyme required to hydrolyze 1 nmol of substrate per min under the conditions of the assay.

The aminopeptidase activity of $APEH_{Ss}$ was measured by using acetyl-amino acid-*p*NA, such as acetyl-Leu-*p*NA (0.1 mM) (Sigma) and acetyl-Ala-*p*NA (10 mM) (Bachem), following the standard assay procedure described above. Unless otherwise reported, Suc-GlyGlyPhe-*p*NA was the substrate used to measure the protease activity. All experiments were carried out in triplicate on two different protein preparations.

Temperature, pH, $CaCl_2$ and SDS effects on $APEH_{Ss}$ activity

Protease activity was measured at different pH values from 4.5 to 9.0 under the assay conditions described above. Citrate/phosphate buffer (50 mM) was used for pH values ranging from 4.5 to 6.5 and Tris-HCl buffer (50 mM) for pH values between pH 7.5 and 9.0. Relative activity was expressed as a percentage of the maximum of the enzyme activities under the standard assay conditions.

pH stability was tested by 30 min incubation of the purified enzyme in appropriate buffers at 80 °C. The activity of $APEH_{Ss}$ as a function of SDS concentration was performed by pre-incubation the enzyme with the detergent (0–0.24 mM) at 80 °C before the addition of the substrate.

Kinetic constant determination

The kinetic parameters of $APEH_{Ss}$ were determined at 80 °C and all experiments were carried out in triplicate on two different protein preparations. The assays were performed using the chromogenic substrates and the procedures mentioned above. Data were fitted to the Michaelis–Menten equation by a nonlinear regression with the GraphPad Prism software.

Serine protease inhibitory activity of SsCEI wild type and mutants

The inhibition constants Ki were determined by the Lineweaver–Burk equation $\{1/V = 1/V_{max} + (K_m/V_{max})^* (1 + I/K_i)\ ^*1/S\}$. Each reaction mixture, containing SsCEI and the target protease, was pre-incubated at 80 °C for 30 min and the samples were sub sampled and assayed with increasing concentrations of the selected protease substrates Ac-Leu-*p*NA (0.05–0.3 mM) or Suc-GlyGlyPhe-*p*NA (0.03–0.4 mM) in a final volume of 1 mL. All experiments were done in triplicate on two different protein preparations. The IC_{50} values of SsCEI were derived fitting the experimental data with the GraphPad Prism software, through a nonlinear curve-fitting method and using a simple binding isotherm equation $\{\%I = \%I_{max}^*[I]/(IC_{50} + [I])\}$.

The same inhibition experiments were performed using the mutants of SsCEI (M1 L125A/L126S and M2 L126S obtained by Geneart (Regensburg, Germany) and already described by Palmieri *et al.*[6]

The IC_{50} value of SsCEI was determined towards APEH from porcine liver (TaKaRa) using Ac-Leu-pNA (250 μM) as protease substrate. The protease (0.003 μM) and increasing concentrations of SsCEI (0.01–0.08 μM) were mixed and pre-incubated for 30 min at 37 °C before the addition of the substrate. The residual enzymatic activity was determined using the assay procedure described above. Data were fitted with the GraphPad Prism software.

Preparation of extracellular and surface-membrane protein fractions

Extracellular proteins from 2.5 L TYS culture medium withdrawn at stationary phase (OD_{600} 1.3), were precipitated by the addition of $(NH_4)_2SO_4$ up to 90% saturation at 4 °C and centrifuged at 12 000 × g for 30 min. The protein pellet was re-suspended in 25 mM Tris-HCl, pH 7.5 and dialyzed against the same buffer overnight at 4 °C. The protein sample was then concentrated by ultra-filtration through Amicon membranes (cut-off 10 kDa).

Surface-membrane protein fraction was prepared by dissolving the cell pellet recovered from TYS cultures at stationary phase (OD_{600} 1.3), in 20 mM Tris-HCl pH 6.5 buffer containing 0.7 mM PMSF followed by disrupting through ultrasonic treatment in the same buffer. Unbroken cells were removed by low-spin centrifugation at 2000 × g at 4 °C for 20 min. The supernatant was ultracentrifuged at 100 000 × g for 45 min at 4 °C. Surface

proteins were extracted in 1% Triton X-100 according to Elferink *et al.*[25]

The obtained surface and extracellular protein fractions were analyzed by 8.0% SDS-PAGE and assayed for APEH activity using Ac-Leu-*p*NA as substrate.

Homology modelling and protein–protein docking

The 3D model of $APEH_{Ss}$ was built using the protein homology/analogy recognition engine PHYRE[26] (version 0.2).

PHYRE server scored $APEH_{Ap}$[12] (PDB code 2HU5) as the best template with a lower *E*-value (2.2×10^{-38}) and 34% sequence identity on the full-length protein of more than 560 amino acids. A careful check of the 3D model built was carried out using the molecular graphic package INSIGHT (Accelrys), in order to verify the occurrence of bugs due to insertions and/or deletions within template secondary-structure elements.

The structural model was refined through energy minimization by a 2000 steps of conjugate gradient minimization using the DISCOVER module of INSIGHT package (Accelrys), with the covalent valence force field (CVFF).

Since biochemical studies reveal that $APEH_{Ss}$ has a dimeric arrangement, the model of the dimer was built using the $APEH_{Ap}$ X-ray dimer[12] as template. In details, two identical $APEH_{Ss}$ model monomers were arranged like the two $APEH_{Ap}$ monomers (chain A and chain B) in the crystal dimer, by simply fitting the Cα atomic coordinates. The obtained dimer model was energy-minimized following the procedure previously described for the monomer.

ZDOCK[27] program was used to predict the docking complex between $APEH_{Ss}$ modelled dimer and SsCEI[6] protein inhibitor. This program has proven to achieve good performances in the CAPRI Challenge[28] in the field of predicting protein–protein complexes. ZDOCK is a fast Fourier transform (FFT)-based, initial-stage rigid-body molecular docking algorithm which employs pair-wise shape complementarities (PSC), desolvation and electrostatics in its calculation. The ZDOCK predicted complexes were filtered according to the involvement of SsCEI region 123–130 into the binding, by using the information derived by the mutagenesis studies herein reported. The selected complexes were further clustered (RMSD on inhibitor Cα atoms of 15 Å) using MOLMOL program[29] and the representative model of the most populated cluster was then chosen as the final predicted complex. The predicted rigid-body complex was later energy minimized to allow geometry relaxation and avoid conformational clashes by performing 1000 steps of CG. The protein–protein interface of the docking complex was further analysed by the PROTORP Protein–protein interface analysis server.[30]

Amino acid sequence alignments were obtained using CLUSTALW.[31] MOLMOL program was employed for molecular visualization and analysis.[29]

Results and discussion

Purification of the endogeneous SsCEI-interacting protease

SsCEI, the first archaeal protease inhibitor isolated from *Sulfolobus solfataricus* P2, shows a strong inhibitory activity against eukaryal serine proteases such as α-chymotrypsin and elastase.[6] Although the structure–function relationship of SsCEI has been studied extensively, relatively little is known about the biological function of the native protein. Therefore, as a first approach we decided to identify the intrinsic protease target(s) of SsCEI by making use of the strong interaction between the protease and its inhibitor. The purified protease was characterized in order to obtain a better understanding of the physiological and evolutionary roles of SsCEI.

An optimized purification procedure was applied, which starts from a crude protein extract of *S. solfataricus* grown on proteinaceous substrate and makes use of SsCEI and the chymotrypsin-like substrate Suc-GlyGlyPhe-*p*NA to detect the protease activity in response to SsCEI-interaction.

By way of a combination of hydrophobic affinity, anion exchange and gel filtration chromatography, the SsCEI-interacting protease was purified about 435-fold from the *S. solfataricus* culture possessing an activity recovery of 23%, as summarized in Table 1. The homogeneity of the final preparation was proved by SDS-PAGE (Fig. 1A) and N-terminal sequence analysis. The amount of purified protease was 0.1 mg and the specific activity was measured as 100 U mg^{-1}.

Identification of a SsCEI-interacting protease

The purified interacting protein was subjected to in-gel digestion and the tryptic peptides analysed by nano-HPLC-ESI-MS/MS. The putative acylaminoacyl-peptidase (apeH-2) product of *sso2141* gene of *S. solfataricus* P2, was identified with 37% sequence coverage (Table S1, ESI†).

A similarity search revealed that SSO2141 possesses 27% sequence identity with the acyl peptide hydrolase (APEH) from *Rattus norvegicus* and *Homo sapiens* in the C-terminal region which includes the catalytic domain. Moreover, sequence identity of SSO2141 with the two previously described archaeal APEHs from *A. pernix*[12] (APE_1547.1) and *P. horikoshii*[16] (PH0863) was approximately 34% and 26%, respectively. The *sso2141* encoded protein consists of 569 amino acids (Fig. 1B) making it smaller than the homologous APEHs from mammalia (from 700 to 800 amino acids) or archaea (from 600 to 700 amino acids). By protein sequence analysis, the first 10 amino acid residues of the N terminus of

Table 1 Purification of SsCEI-interacting protease from 0.5 L of *S. solfataricus* culture

Purification step	Total activity/U	Total protein/mg	Specific activity/U mg^{-1}	Yield (%)	Purification fold
Soluble extract	60	250	0.2	100	1
Phenyl Sepharose	60	33	1.8	100	7.8
Mono Q	44.2	1.2	37	73	160
Superose 12	28	0.5	58.3	46.7	253
Pheyl Superose	14	0.1	100	23	435

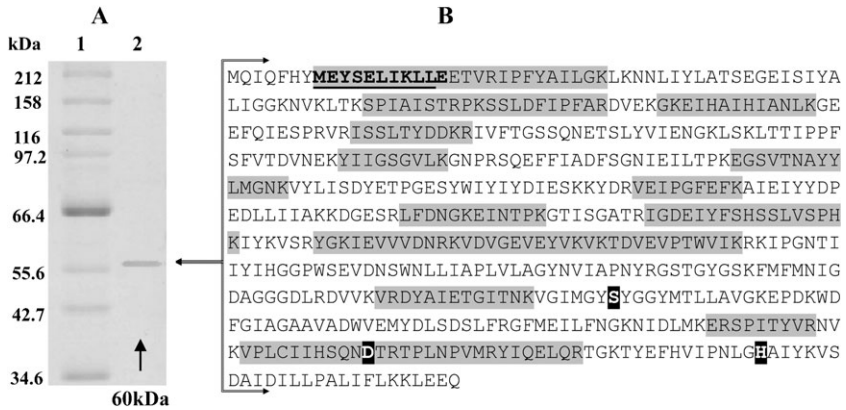

Fig. 1 (A) SDS-PAGE of SsCEI-interacting protease from *Sulfolobus solfataricus*. Lane 1, molecular weight markers (myosin 212 kDa, MBP-β-galactosidase 158 kDa, β-galactosidase 116 kDa, phosphorylase b 97.2 kDa, serum albumin 66.4 kDa, glutamic dehydrogenase 55.6 kDa, MBP2 E. coli 42.7 kDa, thioredoxin reductase 34.6 kDa); lane 2, purified protease. (B) The amino acid sequence deduced from the protease coding *sso2141* gene. The peptides sequenced by MS/MS are highlighted in grey and the conserved locations of the catalytic triad (Ser, Asp and His) in the protein sequence are indicated in black bold. The N-terminal amino acid sequence of the purified protease is underlined in bold. This sequence shows that the protein translation process starts from Met.[8]

SSO2141 were detected as MEYSELIKLL. This sequence was identical to that deduced from the coding gene *sso2141* (Fig. 1B) except for the first seven residues (M^1QIQFHY^7-M^8), suggesting that the protein translation process starts from Met.[8]

Molecular properties and cellular localization of the SsCEI-interacting protease

The molecular mass of the purified protease (60.0 kDa, Fig. S1, ESI†) as determined by SDS-PAGE (Fig. 1A) analysis was consistent with the theoretical value calculated from the amino acid sequence derived from the DNA sequence (63.33 kDa). However, as verified by gel filtration chromatography, the native enzyme had a molecular mass of 125 kDa and consisted of two identical subunits. Therefore the protein is likely to consist of a dimeric structure which is in contrast to the tetramer APEH mammalian counterpart[15,17–19] but in agreement with the structural findings of the archaeal APEHs both from *A. pernix*[12] and *P. horikoshii*.[16]

It is known that acyl-peptide hydrolase catalyzes the hydrolysis of N-terminally acetylated peptide to release *N*-acetyl amino acid.[9] To examine the activity of the purified enzyme from *S. solfataricus*, we used Ac-Leu-*p*NA and Ac-Ala-*p*NA as substrates and the kinetic parameters (Table 2) were determined. At 80 °C and pH 7.5, the purified enzyme exhibited hydrolytic activity *versus* Ac-Leu-*p*NA and Ac-Ala-*p*NA but no activity was detected when Leu-*p*NA and Ala-*p*NA were used as substrates. This protein was therefore concluded to be the APEH from the thermophilic archaeon *S. solfataricus* and it was named $APEH_{Ss}$. As shown in Table 2, $APEH_{Ss}$ shows preference for Ac-Leu-*p*Na over Ac-Ala-*p*Na, which is the classic substrate of APEHs from mammals.[15,17–19,32] The catalytic efficiency values (k_{cat}/K_m) of $APEH_{Ss}$ determined for all the substrates tested are very similar to those reported for the archaeal APEHs from both *A. pernix*[12] and *P. horikoshii*[16] (Table 2). Moreover, $APEH_{Ss}$ shows a Km value for Ac-Leu-*p*NA more or less identical to that obtained for APEH from *A. pernix*,[12] suggesting a common substrate binding mode of the two enzymes for this substrate, which is also confirmed by the identity of all the active site residues. As reported for $APEH_{Ap}$,[12] $APEH_{Ss}$ was able to hydrolyse Suc-GlyGlyPhe-*p*NA, showing endopeptidase activity in contrast to the eukaryal APEHs, which are classic aminopeptidases.[15,17–19]

The enzymatic properties of $APEH_{Ss}$ were characterized. The optimum temperature of the enzyme was 80 °C and the optimum pH at 80 °C was between pH 7.5 and 9.0. Moreover, the activity of $APEH_{Ss}$ decreased with increasing concentrations of $CaCl_2$ or SDS. Specifically, 48% of the relative activity was measured in the presence of 100 mM $CaCl_2$ and no activity was detected at SDS concentrations higher than 0.3 mM, possibly due to overcharging and/or a denaturing action on the enzyme active site. As for thermal stability, the enzyme retained 100% activity after 72 h of incubation both at 50 °C and 70 °C (Fig. S2, ESI†).

In order to determine the cellular localization of $APEH_{Ss}$, extracellular and surface-membrane protein fractions from *S. solfataricus* cell cultures were prepared and assayed using Ac-Leu-*p*Na as the substrate. Results confirmed the cytosolic localization of the *Sulfolobus* protease in agreement with the homologous archaeal[12,16] and eukaryal APEHs.[15,17–19]

Acylpeptide hydrolase inhibitory activity of SsCEI

To investigate the ability of SsCEI to inhibit $APEH_{Ss}$, the enzyme was pre-incubated with the inhibitor at various concentrations and residual enzymatic activity towards the reported substrates Ac-Leu-*p*NA and Suc-GlyGlyPhe-*p*NA was measured. The Lineweaver–Burk plots are shown in Fig. 2. The straight lines obtained at different inhibitor concentrations, all intersecting in one point corresponding to $1/V_{max}$, indicate that the SsCEI acts as a typical competitive inhibitor. Therefore these results demonstrated that an increase in substrate concentration induced a displacement of SsCEI bound to the APEH resulting in EI dissociation. In fact, competitive inhibition is a mechanism where binding of the inhibitor to the active site of the enzyme prevents binding

Table 2 Kinetics parameters of *S. solfataricus* $APEH_{Ss}$ in comparison with those from archaeal and mammalian organisms

Substrate	Enzyme	K_m/mM	k_{cat}/s^{-1}	$(k_{cat}/K_m)/s^{-1}$ mM^{-1}
Ac-Leu-*p*NA	APEH[a] *P. horikoshii*	11.0	3.3×10^2	0.3×10^2
	APEH[b] *A. pernix*	0.4	9.3	0.2×10^2
	APEH *S. solfataricus*	0.3	5.0	0.2×10^2
Suc-GlyGlyPhe-*p*NA	APEH *S. solfataricus*	1.2	2.5	2.1
Ac-Ala-*p*NA	APEH *S. solfataricus*	11.4	5.0	0.4
	APEH[c] Porcine	1.8	4.0×10^3	2.3×10^3
	APEH[a] *P. horikoshii*	18.4	17.3	0.9
	APEH[d] Rat	8.3	1.9×10^3	2.3×10^2

[a] See ref. 16. [b] See ref. 35. [c] See ref. 12;18. [d] See ref. 17,32.

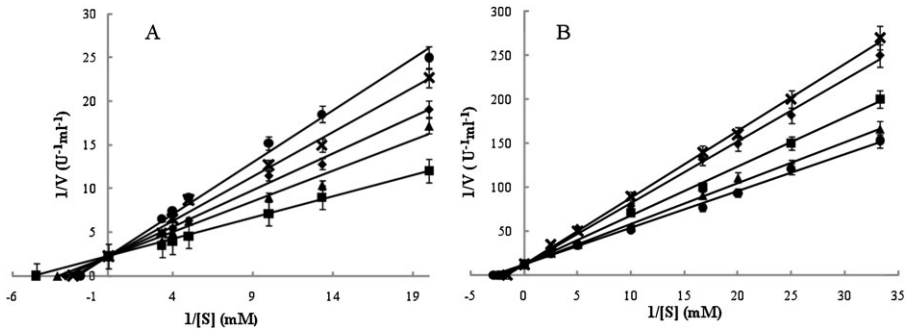

Fig. 2 (A) Inhibition kinetic analysis. $APEH_{Ss}$ (0.003 μM) was incubated without (■) or with SsCEI at 0.014 μM (◆), 0.016 (▲), 0.02 μM (×), and 0.04 μM (●) concentrations and assayed at increasing substrate Ac-Leu-*p*NA concentrations. The reciprocals of the rate of the substrate hydrolysis for each inhibitor concentration were plotted against the reciprocals of the substrate concentrations. K_i was determined from the formula as per the competitive type of inhibition. (B) Inhibition kinetic analysis. $APEH_{Ss}$ (0.007 μM) was incubated without (●) or with SsCEI at 0.005 μM (▲), 0.01 μM (■), 0.014 μM (◆) and 0.03 μM (×) concentrations and assayed at increasing concentrations of Suc-GlyGlyPhe-*p*NA. The reciprocals of the rate of the substrate hydrolysis for each inhibitor concentration were plotted against the reciprocals of the substrate concentrations. The inhibition constants K_i were determined by the Lineweaver–Burk equation $\{1/V = 1/V_{max} + (K_m/V_{max})*(1 + I/K_i) *1/S\}$.

of the substrate and *vice versa* in a dynamic equilibrium-like process. Analysis of the data obtained yielded a dissociation constant (K_i) value of 20 ± 0.001 nM for the SsCEI–$APEH_{Ss}$ complex using both substrates mentioned above (Table 3). This value is slightly lower than the K_i value of 80 nM estimated for the SsCEI -α-chymotrypsin complex.[6] Further inhibition analyses were performed by pre-incubating $APEH_{Ss}$ with increasing amounts of the inhibitor and the half maximal (50%) inhibitory concentration (IC) of SsCEI was calculated. The calibration curve for SsCEI followed a hyperbolic pattern and IC_{50} values were calculated as $0.020 \pm 5.1 \times 10^{-3}$ with Ac-Leu-*p*NA and $0.011 \pm 2.6 \times 10^{-3}$ with Suc-GlyGlyPhe-*p*NA (Table 3 and Fig. S3, ESI†). Surprisingly, despite the thermophilic nature of SsCEI the inhibition activity as a function of temperature revealed slight differences (about 20%) in the temperature range 37–90 °C.

The inhibition activity of SsCEI was also evaluated using mammalian APEH from porcine liver and human intestine. Porcine liver APEH activity was measured by following the hydrolysis of Ac-Leu–*p*NA. The IC_{50} value was calculated as $0.019 \pm 4.4 \times 10^{-3}$ (Table 3). Furthermore, SsCEI exhibited inhibition activity *versus* APEH from human intestinal Caco2 cells (data not shown) and the IC_{50} value seemed to be similar to that determined for APEH from porcine liver (Fig. S3, ESI†).

Table 3 K_i and IC_{50} values relative to inhibition of APEH from *S. solfataricus* and porcin liver by SsCEI

Substrate	Enzyme	K_i/μM	IC_{50}/μM
Ac-Leu-*p*NA	APEH Porcine	N.d.	$0.019 \pm 4.4 \times 10^{-3}$
	APEH *S. solfataricus*	0.02 ± 0.001	$0.020 \pm 5.1 \times 10^{-3}$
Suc-GlyGlyPhe-*p*NA	APEH *S. solfataricus*	0.02 ± 0.001	$0.011 \pm 2.6 \times 10^{-3}$

To obtain insights into the molecular determinants of SsCEI binding towards $APEH_{Ss}$, mutagenesis/inhibition studies were performed using the SsCEI mutants designed in our previous work, M1 (L125A/L126S) and M2 (L126S).[6] Results unambiguously demonstrated that both mutants were unable to inhibit $APEH_{Ss}$, confirming that the already identified reactive site loop of SsCEI was involved in the specific inhibition of $APEH_{Ss}$, similarly to that observed using α-chymotrypsin and elastase as protease targets. These findings have been further used to guide protein–protein docking.

Homology modelling of $APEH_{Ss}$

In order to characterize the endogenous protease target $APEH_{Ss}$ from a structural point of view, a homology model was built up and its interaction with the SsCEI inhibitor investigated through a protein–protein docking approach.

The $APEH_{Ss}$ model was constructed using the crystal structure of the full-length acylaminoacyl peptidase from the hyperthermophile *A. pernix* K1 ($APEH_{Ap}$) as a template.[12] This protein, which is a member of the POP family, displays 34% sequence identity to $APEH_{Ss}$ (Fig. 3), thus leading to a high score model using the PHYRE server.[26]

The sequence identity even increases (up to 46%), if we look at the catalytic domain alone (residues 309–562). As shown in Fig. 3, the homology between $APEH_{Ss}$ and $APEH_{Ap}$ extends over most of the amino acid sequence; the putative catalytic triad Ser425, Asp505, His537 and the oxyanion binding site (Gly349), which are typical of the POP family, are conserved. The consensus sequence Gly-X-Ser-X-Gly, which includes the active site serine residue, is also present in $APEH_{Ss}$. Moreover, almost all of the active site residues involved in substrate binding, as revealed by the crystal structure of $APEH_{Ap}$-inhibitor complexes,[12,13] are conserved. It is noteworthy that residues suggested[32–35] to play key roles in $APEH_{Ap}$ structure stability and/or catalysis, such as Glu88, His367 and Arg526 (numbered according to $APEH_{Ap}$ crystal structure), are preserved.

The 3D structure model of $APEH_{Ss}$ (Fig. 4) has the typical architecture of POP family enzymes, showing a α/β-hydrolase catalytic domain with the catalytic triad covered by the central tunnel of an unusual β-propeller domain. This domain is responsible for enzyme specificity towards short peptides, by excluding large peptides and proteins from the active site. Like in $APEH_{Ap}$, the N-terminal β-propeller domain (residues 17–308) consists of seven blades; each blade is made up of four antiparallel strands. The twisted β-sheets show the classic arrangement of β-propeller structures,[10–13] as they are packed face-to-face and arranged radially around a central axis leading to the formation of the central tunnel. The C-terminal domain (residues 308–562) has a canonical α/β hydrolase fold with a central eight-strand mixed β-sheet, flanked by five helices on one side and six helices on the other. As in $APEH_{Ap}$, a short α-helix at the N-terminus (residues 2–16) extends from the β-propeller domain and forms part of the hydrolase domain. The putative Ser-Asp-His catalytic triad is located at the interface of the two domains, and is covered by the tunnel formed by the N-terminal β-propeller domain. Finally, the model structure indicates two possible entries/exits for substrates/products like in $APEH_{Ap}$, *i.e.* the β-propeller central tunnel and a second smaller side-opening located between

Fig. 3 Amino acid sequence alignment of $APEH_{Ss}$ and $APEH_{Ap}$. Different symbols have been used to represent identical amino acid residues (*), conserved substitutions (:) and semi-conserved substitutions (.) between the two proteins. Significant residues have been underlined in colour (bold letters: catalytic triad; yellow: active site residues; green: oxyanion binding pocket; grey: residues belonging to the dimer interface).

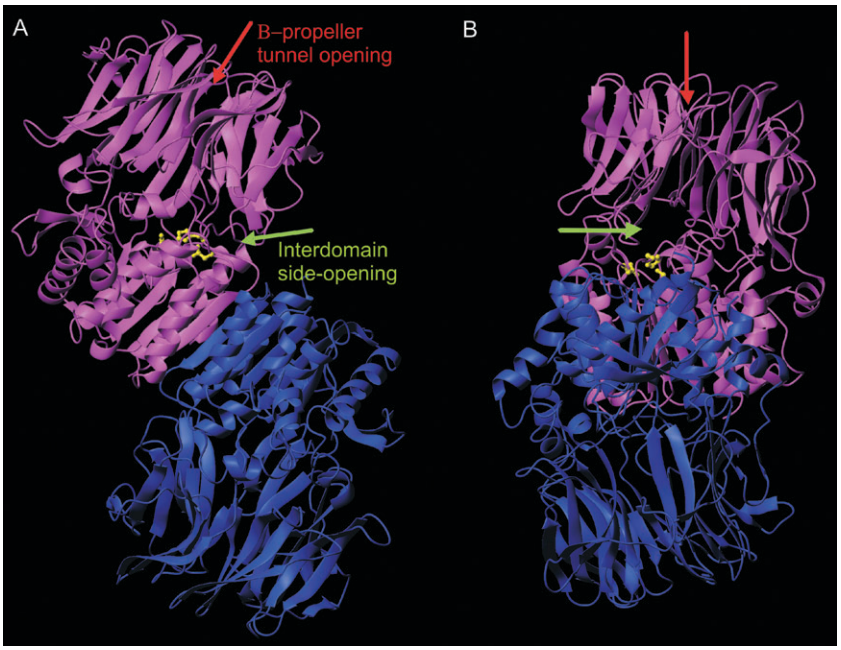

Fig. 4 $APEH_{Ss}$ dimer model. The two monomeric subunits are displayed in different colours as cartoon. (A) For only one of the two subunits the catalytic triad residues (Ser425, Asp505, His537) are shown in yellow (ball-and-stick mode); the red and green arrows indicate the β-propeller tunnel opening and the interdomain side-opening, respectively. (B) View rotated 90° along the *z*-axis (vertical axis parallel to the image plane).

blades 1 and 2 in the interdomain region (Fig. 4). Although it has been previously hypothesized that the former and latter routes could represent the substrate entry and/or the product exit, respectively, the detailed catalytic mechanism of the enzyme remains to be elucidated.[11,13] Since biochemical analysis indicated that native $APEH_{Ss}$ exists in a dimeric form in agreement to that revealed for the APEHs isolated both from *A. pernix*[12] and *P. horikoshii*,[16] we put forward the hypothesis for the dimeric arrangement of $APEH_{Ss}$ (Fig. 4), using *A. pernix* crystal structure as a template.[12] The sequence alignment analysis between APEHs from *A. pernix* and *S. solfataricus* shows that the residues at the dimer interface are conserved (Fig. 3). This evidence suggests a common mode of dimer formation. In particular, residues involved in side

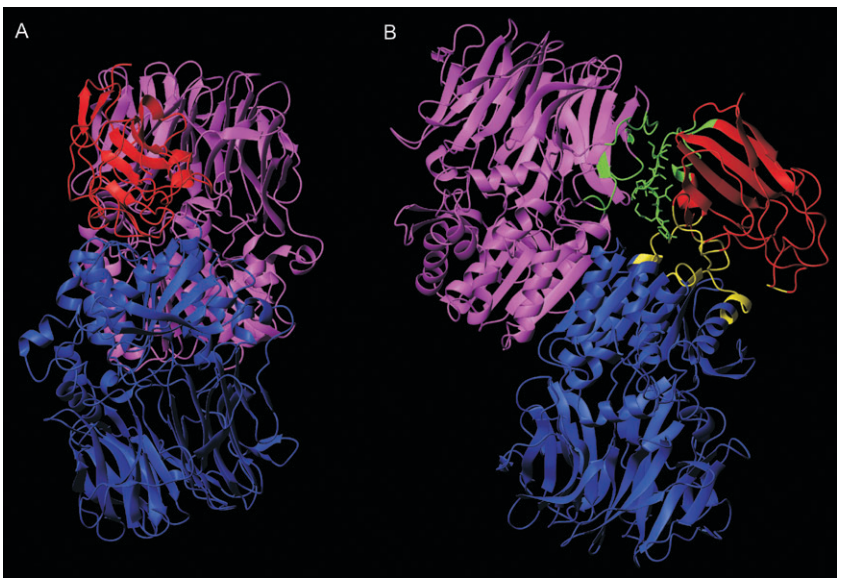

Fig. 5 (A) Model complex between $APEH_{Ss}$ dimer and SsCEI (shown in red) (same orientation as in Fig. 4B). (B) Interacting regions are displayed in colours (same orientation as in Fig. 4A). Two different colours (green and yellow) have been used to distinguish the contributions of the two $APEH_{Ss}$ monomeric subunits to the complex interface. $APEH_{Ss}$ green regions: 51, 54–56, 74–78, 92–101, 538–539; $APEH_{Ss}$ yellow regions: 406–417, 439–443, 494–496, 559–562. The corresponding SsCEI interacting regions have been coloured according to the same colour scheme; SsCEI green regions: 46, 122–129, 139–147; SsCEI yellow regions: 25–26, 82–86, 92–98, 130–133. The SsCEI region 123–130 is displayed in stick-form.

chain hydrogen bonds between the two monomers in the $APEH_{Ap}$ X-ray structure are retained (like S10, E17 and Q522 numbered according to *A. pernix* crystal structure). In the $APEH_{Ss}$ symmetric dimer, the two subunits are related by a 2-fold rotation axis, and the dimer interface is located exclusively in the C-terminal hydrolase domain (Fig. 4).

The structural similarity between the $APEH_{Ss}$ model and its homologous from *A. pernix*, in particular in the nearby of the active site, is consistent with the biochemical studies herein reported, which indicate a highly comparable enzyme activity for the two APEHs.

Proposed model of the $APEH_{Ss}$–SsCEI complex

To gain insights into the interaction of $APEH_{Ss}$ and its protein inhibitor SsCEI, a protein–protein docking analysis was performed using the $APEH_{Ss}$ dimer model built herein, and the SsCEI structural model previously reported.[6] The ZDOCK algorithm[27] was employed for rigid-body protein–protein docking simulations. The ZDOCK predicted complexes were filtered using the information derived by the mutagenesis studies, indicating the involvement of the SsCEI reactive site loop encompassing the residues L125–L126 in the interaction with the enzyme target. In the predicted complex model (Fig. 5), SsCEI interacts with both monomers of $APEH_{Ss}$ by closing the receptor interdomain side-opening. The comparison between Fig. 4 (panel B) and Fig. 5 (panel A) clearly shows the closure of the enzyme side-opening upon inhibitor binding. A graphical picture of interface protein regions is depicted in Fig. 5. Analysis of the electrostatic potential surfaces (EPSs) of the enzyme and the inhibitor reveals that the enzyme β-propeller tunnel opening is surrounded by a wide region of negative potential (Fig. S4, ESI†). This could be the reason for which the inhibitor does not prefer to interact with the receptor β-propeller opening, since it does not possess wide positively charged surface patches. The predicted model complex indicates that the inhibitor acts through a mechanism of steric-blockage of the enzyme, disallowing the substrate access to the active site or the product release, depending on whether the interdomain side-opening represents the pathway for entering or exiting the active site, respectively. Moreover, it suggests that the interdomain side-opening plays a key role in the catalytic mechanism. This suggestion does not conflict with the experimental data relating to other members of the POP family representing the interdomain region directly involved in the substrate entry mechanism.[36–39] In fact, in the case of DPPIV[36,40] (dipeptidyl peptidase IV), protease substrates can access the active site through the interdomain region which consists of a large side opening. Moreover, by crystallographic studies,[10,37] both a "closed" (similar to our $APEH_{Ss}$ structural model) and an "open" conformation have been detected in other POP family members. In the "open" conformation, loops connecting the peptidase and propeller domains act like a hinge allowing the domains to move apart, creating a large interdomain opening which could easily accommodate substrates. In our previous work it was suggested that the SsCEI inhibitor behaves like a mechanism-based inhibitor toward α-chymotrypsin and elastase.[6] Indeed, the APEH molecular structure is very different from canonical serine proteases since the active site is not solvent exposed and cannot be reached by the protein inhibitor. Thus, it would not be so surprising that the same inhibitor uses different mechanisms since the enzyme targets are very different, from both a structural and a functional point of view. On the other hand, it cannot be excluded that APEH undergoes a conformational change during inhibitor binding, leading to exposure of binding site residues to the incoming protein inhibitor, allowing for a different inhibitor binding mode. The latter case cannot be taken into account with the rigid-body docking approach employed in the present work. However, even in this case our predicted complex could at least provide some hints in relation to the early stages of protein inhibitor approach. The binding of only one inhibitor molecule has been discussed; however, the proposed complex model reveals that the simultaneous binding of two SsCEI molecules to the receptor dimer is also allowed (Fig. S5, ESI†).

Conclusions

In summary, our work reports on the identification and characterization of an APEH from *S. solfataricus* and the analysis of its binding to SsCEI by biochemical and modeling studies. To the best of our knowledge this is the first time that a specific and selective interaction between a PEBP protein such as SsCEI and a protease member of the acylpeptide hydrolase is reported. Preliminary data on SsCEI inhibition activity show that it efficiently inhibits mammalian APEHs, including the human isoform. This finding is extremely remarkable since it has been suggested that deficiencies or changes at the genetic and protein levels of members of this protease family, are associated with a number of disorders in human including Alzheimer's disease[41,42] and cancer.[20–22] Thus, the discovery of a specific inhibitor of APEH represents a valuable starting point for the design of small bioactive molecules able to "knock out" acylpeptide hydrolase activity and acting as new promising pharmacological drugs.

Acknowledgements

The authors wish to thank Mr Luca De Luca for technical support.

References

1 U. Hengst, H. Albrecht, D. Hess and D. Monard, *J. Biol. Chem.*, 2001, **276**, 535–540.
2 J. Mima, Y. Narita, H. Chiba and R. Hayashi, *J. Biol. Chem.*, 2003, **278**, 29792–29800.
3 B. S. Vallee, P. Tauc, J. C. Brochon, R. Maget-Dana, D. Lelievre, M. H. Metz-Boutigue, N. Bureaun and F. Schoentgen, *Eur. J. Biochem.*, 2001, **268**, 5831–5841.
4 K. Yeung, T. Seitz, S. Li, P. Janosch, B. McFerran, C. Kaiser, F. Fee, K. D. Katsanakis, D. W. Rose, H. Mischak, J. M. Sedivy and W. Koich, *Nature*, 1999, **401**, 173–177.
5 A. W. Bruun, I. Svendsen, S. O. Sorensen, M. C. Kielland-Brandt and J. R. Winther, *Biochemistry*, 1998, **37**, 3351–3357.
6 G. Palmieri, G. Catara, M. Saviano, E. Langella, M. Gogliettino and M. Rossi, *J. Proteome Res.*, 2009, **8**(1), 327–334.
7 L. Polgar, *Cell. Mol. Life Sci.*, 2002, **59**, 349–362.
8 N. D. Rawlings, L. Polgar and A. J. Barrett, *Biochem. J.*, 1991, **279**, 907–908.

9 W. M. Jones, A. Scaloni and J. M. Manning, *Methods Enzymol.*, 1994, **244**, 227–231.
10 V. Fülöp, Z. Böcskei and L. Polgar, *Cell*, 1998, **94**(2), 161–170.
11 D. Rea and V. Fülöp, *Cell Biochem. Biophys.*, 2006, **44**, 349–365.
12 A. L. Kiss, B. Hornung, K. Rádi, Z. Gengeliczki, B. Sztáray, T. Juhász, Z. Szeltner, V. Harmat and L. Polgár, *J. Mol. Biol.*, 2007, **368**, 509–520.
13 M. Bartlam, G. Wang, H. Yang, R. Gao, X. Zhao, G. Xie, S. Cao, Y. Feng and Z. Rao, *Structure*, 2004, **12**, 1481–1488.
14 W. Gade and J. L. Brown, *J. Biol. Chem.*, 1978, **253**, 5012–5018.
15 K. K. Sharma and B. J. Ortwerth, *Eur. J. Biochem.*, 1993, **216**, 631–637.
16 K. Ishikawa, H. Ishida, Y. Koyama, Y. Kawarabayasi, J. Kawahara, E. Matsui and I. Matsui, *J. Biol. Chem.*, 1998, **273**, 17726–17731.
17 K. Kobayashi and J. A. Smith, *J. Biol. Chem.*, 1987, **262**, 11435–11445.
18 V. Raphel, T. Giardina, L. Guevel, J. Perrier, L. Dupuis, X.-J. Guo and A. Puigserver, *Biochim. Biophys. Acta, Protein Struct. Mol. Enzymol.*, 1999, **1432**, 371–381.
19 A. Scaloni, W. M. Jones, D. Barra, M. Pospischil, S. Sassa, A. Popowicz, L. R. Manning, O. Schneewind and J. M. Manning, *J. Biol. Chem.*, 1992, **267**, 3811–3818.
20 A. Scaloni, W. Jones, M. Pospischil, S. Sassa, O. Schneewind, A. M. Popowicz, F. Bossa, S. L. Graziano and J. M. Manning, *J. Lab. Clin. Med.*, 1992, **120**(4), 505–506.
21 R. Erlandsson, F. Boldog, B. Persson, E. R. Zabarousky, R. L. Allikmets, J. Sümegi, G. Klein and H. Jörnvall, *Oncogene*, 1991, **6**, 1293–1295.
22 S. L. Naylor, A. Marshall, C. Hensel, P. F. Martinez, B. Holley and A. Y. Sakaguchi, *Genomics*, 1989, **43**, 55–361.
23 P. G. Richards, M. K. Johnson and D. R. Ray, *Mol. Pharmacol.*, 2000, **58**, 577–583.
24 A. Shevchenko, H. Tomas, J. Havlis, J. V. Olsen and M. Mann, *Nat. Protoc.*, 2006, **1**(6), 2856–2860.
25 M. G. Elferink, S. V. Albers, W. N. Konings and A. Driessen, *Mol. Microbiol.*, 2001, **39**(6), 1494–1503.
26 L. A. Kelley and M. J. E. Sternberg, *Nat. Protoc.*, 2009, **4**, 363–371.
27 R. Chen, L. Li and Z. Weng, *Proteins: Struct., Funct., Genet.*, 2003, **52**, 80–87.
28 K. Wiehe, B. Pierce, W. W. Tong, H. Hwang, J. Mintseris and Z. Weng, *Proteins: Struct., Funct., Bioinf.*, 2007, **69**, 719–725.
29 R. Koradi, M. Billeter and K. Wüthrich, *J. Mol. Graphics*, 1996, **14**, 51–55.
30 C. Reynolds, D. Damerell and S. Jones, *Bioinformatics*, 2009, **25**, 413–414.
31 M. A. Larkin, G. Blackshields, N. P. Brown, R. Chenna, P. A. McGettigan, H. McWilliam, F. Valentin, I. M. Wallace, A. Wilm, R. Lopez, J. D. Thomson, T. J. Gibson and D. G. Higgins, *Bioinformatics*, 2007, **23**, 2947–2948.
32 A. L. Kiss, Z. Szeltnera, V. Fulop and L. Polgar, *FEBS Lett.*, 2004, **571**, 17–20.
33 G. Yang, A. Bai, L. Gao, Z. Zhang, B. M. Zheng and Y. Feng, *Biochim. Biophys. Acta, Proteins Proteomics*, 2009, **1794**, 94–102.
34 A. L. Kiss, A. Palló, G. Náray-Szabó, V. Harmat and L. Polgár, *J. Struct. Biol.*, 2008, **162**, 312–323.
35 Q. Wang, G. Yangm, Y. Liu and Y. Feng, *J. Biol. Chem.*, 2006, **281**, 18618–18625.
36 H. B. Rasmussen, S. Branner, F. C. Wiberg and N. Wagtmann, *Nat. Struct. Biol.*, 2003, **10**, 19–25.
37 L. Shan, I. I. Mathews and C. Khosla, *Proc. Natl. Acad. Sci. U. S. A.*, 2005, **102**, 3599–604.
38 M. Fuxreiter, C. Magyar, T. Juhász, Z. Szeltner, L. Polgár and I. Simon, *Proteins: Struct., Funct., Bioinf.*, 2005, **60**, 504–512.
39 T. Juhász, Z. Szeltner, V. Fülöp and L. Polgár, *J. Mol. Biol.*, 2005, **346**, 907–917.
40 K. Aertgeerts, S. Ye, M. G. Tennant, M. L. Kraus, J. Rogers, B. C. Sang, R. J. Skene, D. R. Webb and G. S. Prasad, *Protein Sci.*, 2004, **13**, 412–21.
41 R. Yamin, C. Zhao, P. B. O'Connor, A. C. McKee and C. R. Abraham, *Mol. Neurodegener.*, 2009, **4**, 33.
42 C. Olmos, R. Sandoval, C. Rozas, S. Navarro, U. Wyneken, M. Zeise, B. Morales and F. Pancetti, *Toxicol. Appl. Pharmacol.*, 2009, **238**, 37–46.